Zeolite Nanosheet Synthesis (2)

International Edition: DOI: 10.1002/anie.201609983
German Edition: DOI: 10.1002/ange.201609983

Non-Topotactic Transformation of Silicate Nanolayers into Mesostructured MFI Zeolite Frameworks During Crystallization

*Zachariah J. Berkson, Robert J. Messinger, Kyungsu Na, Yongbeom Seo, Ryong Ryoo, and Bradley F. Chmelka**

crystallization · dynamic nuclear polarization · layered silicates · solid-state NMR spectroscopy · zeolites

In a recent Communication in this journal,[1] we reported on the co-development of crystalline and mesoscopic order during the hydrothermal synthesis of mesostructured MFI zeolite nanosheets. Combined X-ray diffraction (XRD), transmission electron microscopy (TEM), and solid-state nuclear magnetic resonance (NMR) spectroscopy analyses provided evidence for the transformation of a nanolayered silicate intermediate into mesostructured MFI zeolite frameworks. Goesten, et al.[26] have raised questions about the interpretations of the experimental results and their bearing on the overall conclusions with respect to the crystallization of the MFI nanosheets. A primary issue is whether zeolite crystallization can proceed through non-topotactic rearrangement of framework bonds. They suggest that the nanolayered silicate species present during the intermediate stages of the MFI nanosheet synthesis are an "artifact" and play no role in the subsequent crystallization of the MFI zeolite product. They assert that the MFI zeolite nanosheets crystallize through dissolution of the initially formed mesostructured (non-crystalline) silica and the nanolayered silicate, followed by subsequent reprecipitation of the MFI zeolite nanosheets. While Goesten, et al. acknowledge that the 2D ^{29}Si{^{29}Si} NMR results show that the nanolayered silicate and MFI zeolite domains are "*clearly simultaneously present*," they contend that "*nothing tells us that they are transforming within the same domains.*" Furthermore, they consider it unlikely that the nanolayered silicate intermediate could rearrange structurally without dissolution to form the MFI zeolite frameworks because the structures of the two are dissimilar. The representative TEM and SEM images in Figures 1c, 3, and 4b reported in Messinger, et al.[1] are dismissed as showing "*two different phases on top of each other rather than 'sheets in transformation'*." Finally, they observed more rapid crystallization rates of the mesostructured MFI zeolite nanosheets than reported in Messinger, et al. and saw no evidence for the nanolayered silicate intermediate under their synthetic and characterization conditions.

Herein, we respond to each of the points raised by Goesten, et al.[26] and provide additional evidence that corroborates the analyses and strengthens the conclusions that, under the synthetic conditions used in Messinger, et al.,[1] the crystallization of MFI zeolite nanosheets proceeded predominantly via a nanolayered silicate intermediate. While Goesten, et al. observe that such non-topotactic transformations have been "rare" in the past, there has until now been a lack of experimental probes capable of detecting such subtle molecular rearrangements. However, such challenges are overcome by 2D ^{29}Si{^{29}Si} NMR techniques which provide information on the atomic-level interactions of dipolar- and *J*-coupled pairs of ^{29}Si nuclear spins, whose local (<1 nm) bonding environments are manifested by their respective isotropic chemical shifts. In one-dimensional (1D) NMR spectra, such as 1D ^{29}Si{^{1}H} cross-polarization (CP) magic-angle spinning (MAS) spectra, the ^{29}Si isotropic shifts often overlap, as is the case for the heterogeneous

[*] Z. J. Berkson, Prof. Dr. B. F. Chmelka
Department of Chemical Engineering, University of California
Santa Barbara, CA 93106 (USA)
E-mail: bradc@engineering.ucsb.edu
Prof. Dr. R. J. Messinger
Department of Chemical Engineering
The City College of New York, CUNY
New York, NY 10031 (USA)
Prof. Dr. K. Na
Department of Chemistry, Chonnam National University
Buk-gu, Gwangju, 61186 (Republic of Korea)
Dr. Y. Seo
Department of Chemical & Biomolecular Engineering
University of Illinois at Urbana-Champaign
Urbana, IL 61801 (USA)
Prof. Dr. R. Ryoo
Department of Chemistry, Korea Advanced Institute of Science and Technology, Center for Nanomaterials and Chemical Reactions
Institute for Basic Science
Daejeon 305-701 (Republic of Korea)

Supporting information (Experimental details, low-temperature effects on ^{29}Si chemical shifts of the nanolayered silicate, and 2D ^{29}Si{^{29}Si} *J*-mediated NMR spectrum of a physical mixture of the nanolayered silicate and 13-day MFI zeolite nanosheet product) for this article can be found under: http://dx.doi.org/10.1002/anie.201609983.

intermediate and final mesostructured MFI zeolite products. Goesten, et al. provide 1D $^{29}Si\{^{1}H\}$ CP-MAS NMR spectra to support their contentions,[26] though such low-resolution 1D NMR measurements are ambiguous.

By comparison, the 2D $^{29}Si\{^{29}Si\}$ NMR spectra reported herein and in Messinger, et al.[1] provide significantly higher spectral resolution that yield direct information on the local chemical environments and interconnectivities of ^{29}Si framework moieties. These insights are achieved by correlating the isotropic chemical shifts of pairs of ^{29}Si framework sites that are dipole-dipole-coupled through space or *J*-coupled through ^{29}Si-O-^{29}Si covalent bonds. Of these two interactions, dipole-dipole couplings are stronger and vary as the inverse cube of the separation distance between ^{29}Si nuclei. Such couplings in silicates tend to be localized over distances of less than 1 nm,[2,3] which correspond to nearest or next-nearest tetrahedral (T) site neighbors of ^{29}Si nuclei in silicates and zeolites. 2D $^{29}Si\{^{29}Si\}$ NMR spectra are typically presented as contour plots with two ^{29}Si chemical shift axes, where pairs of 2D signal intensity from ^{29}Si nuclei are correlated across the spectrum diagonal. Such correlated signal intensities in 2D dipolar-mediated $^{29}Si\{^{29}Si\}$ NMR spectra thus identify pairs of dipole-dipole-coupled ^{29}Si nuclei within 1 nm of each other or, in 2D *J*-mediated spectra, pairs of *J*-coupled ^{29}Si nuclei that are connected via covalent (e.g., ^{29}Si-O-^{29}Si) bonds.

The nanoscale proximities of the transforming nanolayered silicate and MFI zeolite frameworks are established by 2D dipolar- and *J*-mediated $^{29}Si\{^{29}Si\}$ NMR spectra of intermediate products obtained at different stages of hydrothermal synthesis. We show in Figure 1 a the same spectrum as in Figure 4 a of Messinger, et al.,[1] which we have modified to emphasize the atomic-level interactions between ^{29}Si sites 1, 2, and 3 in the transforming nanolayered silicates with the ^{29}Si Q^4 sites in the developing MFI zeolite framework after 10 days under hydrothermal conditions at 130 °C. Significantly, the correlated signal intensities from the crystallizing nanolayered silicates are displaced by approximately 0.5 ppm (red dashed lines in Figure 1 a) and appear as shoulders alongside the signals at −96.6, −100.7, −103.3, −108.8, and −114.9 ppm (blue dashed lines in Figure 1 a) from the five resolved ^{29}Si sites in the nanolayered silicates, which have been previously characterized and assigned.[4,5] These displacements in the ^{29}Si signals establish that the local bonding environments of the nanolayered silicates are transforming and, as they do so, are correlated with Q^4 ^{29}Si signals (pink band in Figure 1 a) that are in the spectral region −110 to −114 ppm of MFI zeolite frameworks that is distinct from any of the Q^4 nanolayered silicate signals (specifically sites 4 and 5 at −108.8 and −114.9 ppm). The displaced signals are associated with regions of the nanolayered silicate frameworks that are rearranging to form mesostructured MFI zeolite frameworks, consistent with the 2D *J*-mediated NMR and electron microscopy results discussed below. Dissolution and recrystallization would produce physical mixtures of macroscopically separated nanolayered silicate and MFI zeolite species that would generally be distant from each other and result in negligible correlated intensity in the 2D $^{29}Si\{^{29}Si\}$ NMR spectra, contrary to the assertion by Goesten, et al.[26] that such commingled phases would be "*apt to magnetization transfer in the 2D NMR experiment*."

That the transforming nanolayered silicate and MFI zeolite frameworks are covalently bonded and accompanied by non-topotactic transformation of their structures is confirmed by the 2D *J*-mediated $^{29}Si\{^{29}Si\}$ NMR spectra in Figures 1 b, 2, and 3 a. In contrast to the relatively strong dipole-dipole interactions (ca. 200 Hz), through-bond *J* interactions are an order-of-magnitude weaker (ca. 10–15 Hz),[3,6] so that the distances probed by 2D $^{29}Si\{^{29}Si\}$ *J*-mediated NMR experiments are shorter (ca. 0.5 nm), in practice being sensitive principally to ^{29}Si-O-^{29}Si nearest-neighbor T site pairs.[7] Till now, the weak *J* interactions and low natural isotopic abundance of ^{29}Si (4.7 %), have made solid-state 2D *J*-mediated $^{29}Si\{^{29}Si\}$ NMR spectra of ^{29}Si-O-^{29}Si through-bond connectivities infeasible to acquire without expensive isotopic enrichment of ^{29}Si.

However, recent advances in solid-state NMR spectroscopy, most notably dynamic-nuclear-polarization (DNP)-enhanced MAS NMR techniques at low temperatures (ca. 100 K),[8–11] provide significantly enhanced NMR signal sensitivity that allows the detection and analysis of heteroatom and ^{29}Si environments[12–16] in zeolites at natural abundance ^{29}Si. These advances enable the detection and correlation of ^{29}Si signals from dilute covalently bonded ^{29}Si-O-^{29}Si moieties in the intermediate products of MFI zeolite crystallization. This is demonstrated, for example, by the 2D DNP-enhanced *J*-mediated $^{29}Si\{^{29}Si\}$ spectrum in Figure 1 b of the same intermediate sample (10 days) as measured in Figure 1 a (and Figure 4 a in Messinger, et al.[1]), the integrity of which was verified by XRD and NMR measurements and were the same as previously reported in Ref. [1]. All of the intensity in the 2D *J*-mediated spectrum arises from pairs of covalently bonded (through bridging oxygen atoms) *J*-coupled ^{29}Si nuclei, whose isotropic chemical shifts are correlated across the spectrum diagonal (black dashed line in Figure 1 b). The low temperature conditions required for the DNP-NMR measurements result in broader and slightly displaced ^{29}Si signals at 95 K, owing to the freezing of motions of the diquaternary-ammonium structure-directing species,[7] compared to the dipolar-mediated spectra acquired at 298 K, which otherwise do not affect ^{29}Si-O-^{29}Si framework connectivities.

Nevertheless, multiple covalent connectivities among distinct nanolayered silicate and MFI zeolite moieties are resolved in the 2D DNP-enhanced *J*-mediated $^{29}Si\{^{29}Si\}$ spectrum of Figure 1 b. As in Figure 1 a, the 2D *J*-mediated spectrum shows broad correlated intensity that straddles the diagonal over the range −107 to −116 ppm, which arises from overlapping signals associated with covalently bonded ^{29}Si-O-^{29}Si moieties among the 24 crystallographically distinct Q^4 sites of the MFI zeolite frameworks. The advantages of the 2D NMR results are evident in the high spectral resolution that is obtained, even at 95 K, from locally ordered pairs of *J*-coupled, and therefore covalently bonded, ^{29}Si-O-^{29}Si moieties. Specifically, pairs of correlated signals at −102.4, −109, and −113 ppm are observed between the distinct ^{29}Si sites in the nanolayered silicates (blue lines in Figure 1 b), which are consistent with previously published results, including the

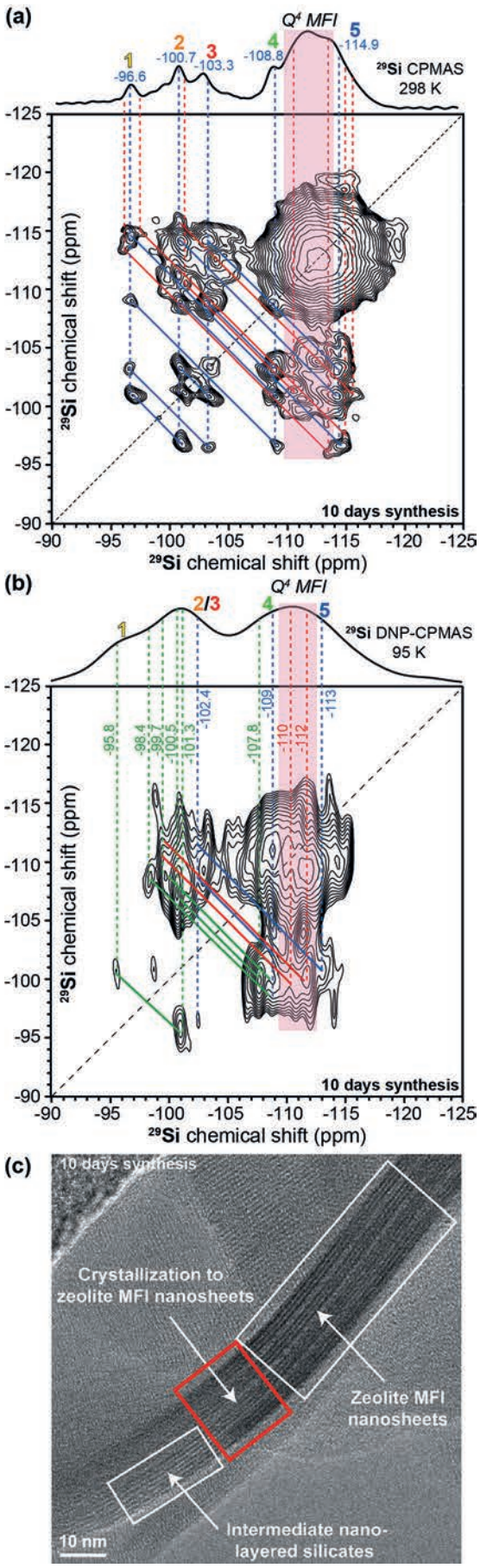

known temperature dependencies of the chemical shifts[7] and site connectivities.[4,5,17] The signals from sites 2 and 3 of the nanolayered silicates overlap at 95 K (Supporting Information, Figure S1), due to inhomogeneous broadening of the signals at low temperature (< 253 K).[7] Well-resolved 2D ^{29}Si signals are also present at −95.8, −98.4, −99.7, −100.5, and −101.3 ppm, with distributions of intensity that reflect similar, but distinct, framework bonding environments that are associated with transforming sites 1, 2, and 3 of the nanolayered silicate (green lines in Figure 1 b). Importantly, these latter signals exhibit intensity correlations with 2D maxima at −107.8 from transforming site 4 moieties and at −110 and −112 ppm from Q^4 ^{29}Si species in the crystallizing MFI zeolite frameworks (red lines in Figure 1 b). Notably, a physical mixture of bulk neat nanolayered silicate and bulk MFI zeolite nanosheet product after 13 days crystallization yields no such intensity correlations in a similar 2D spectrum (Supporting Information, Figures S2 and S3). The 2D *J*-mediated NMR results thus unambiguously establish that ^{29}Si species in the transforming nanolayered silicates are covalently bonded to the crystallizing MFI zeolite frameworks.

If the MFI zeolite frameworks formed only through dissolution and reprecipitation, as suggested by Goesten, et al.,[26] the nanolayered silicate and MFI zeolite moieties would not be covalently bonded to any significant extent. The presence of the *J*-mediated ^{29}Si signals in Figure 1 b is instead consistent with the non-topotactic rearrangement of nanolayered silicates to form the MFI zeolite frameworks. The regions over which such transformations occur are sufficiently numerous and large that they can be resolved in the representative TEM image shown in Figure 4 b of Messinger, et al.,[1] which we have modified in Figure 1 c to emphasize a region in which nanolayered silicate species are rearranging into mesostructured MFI zeolite nanosheets (red box in Figure 1 c). In their counter arguments with respect to the TEM images, Goesten, et al., are partly correct that "*distances of more than 10 nm, with a region of transition in between*" are too large for ^{29}Si *J* couplings to occur between such mesoscopically separated (untransformed) nanolayered silicate and MFI zeolite domains. However, they overlook that the transition domains (such as that depicted in the red-boxed region) contain many rearranging ^{29}Si-O-^{29}Si moieties, which are well within the approximately 0.5 nm needed for effective *J* coupling. The dimensions of the transition regions (separating untransformed nanolayered silicate from crystalline MFI zeolite domains) are relevant only insofar as they are

Figure 1. a) Solid-state 2D dipolar-mediated (through-space, < 1 nm) ^{29}Si{^{29}Si} correlation spectrum of the intermediate product of crystallizing MFI zeolite nanosheets after 10 days of hydrothermal synthesis (modified from Ref. [1]). The spectrum was acquired at 11.7 T, 298 K, and 12.5 kHz MAS. b) Solid-state 2D DNP-enhanced *J*-mediated (through-bond) ^{29}Si{^{29}Si} correlation spectrum, acquired at 9.4 T, 95 K, 8 kHz MAS, in the presence of 16 mM TEKPol biradical in frozen tetrachloroethane (DNP solvent), and under microwave irradiation at 263 GHz. Pairs of correlated signals are indicated by the solid blue, red, and green anti-diagonal lines. c) Representative TEM image showing a region in which intermediate nanolayered silicate sheets are transforming into MFI zeolite nanosheets (modified from Ref. [1]).

sufficiently large and numerous to contain a detectable number of transforming ^{29}Si-O-^{29}Si moieties within the sample (which the 2D *J*-mediated ^{29}Si{^{29}Si} spectra clearly show to be the case). The 2D ^{29}Si{^{29}Si} NMR and TEM results provide complementary and consistent information over their complementary length scales, despite Goesten, et al.'s assertion to the contrary.

The transformation of the intermediate nanolayered silicate species into mesostructured MFI zeolite frameworks is also evident in 2D NMR and microscopy measurements of the products formed at later and earlier stages of hydrothermal synthesis under identical conditions to those used above. The solid-state 2D *J*-mediated ^{29}Si{^{29}Si} NMR spectrum in Figure 2 of the final mesostructured MFI zeolite nanosheet product after 13 days of hydrothermal synthesis (prepared with 99% isotopic ^{29}Si enrichment for increased sensitivity) shows broad correlated intensity across the diagonal in the region −109 to −117 ppm that arises from covalently connected ^{29}Si-O-^{29}Si pairs of Q^4 sites within the MFI zeolite framework. The red band indicates the subportion of this spectral region that does not overlap with any of the nanolayered silicate signals. Individual ^{29}Si resonances associated with the 24 crystallographically distinct ^{29}Si T-sites within the MFI zeolite structure largely overlap, though several are partially resolved, as indicated by the correlated 2D intensity maxima labeled by Roman numerals *x–xii* (orange lines) in Figure 2, which are consistent with previous 2D NMR analyses of bulk MFI zeolite.[18] The 2D spectrum also reveals narrow ^{29}Si signals at −99.7, −101.1, −102.5, and −103.6 ppm, which are attributed to locally ordered Q^3 sites on the mesopore surfaces of the MFI nanosheets, that are correlated with intensity in the range of −114 to −115 ppm (orange lines, Roman numerals *iv–vi*; Figure 2), which corresponds to covalently bonded Q^4 sites within the MFI zeolite nanosheets. Additional narrow ^{29}Si signals are resolved at −105.5, −106.7, and −107.5 ppm that are attributed to locally ordered sub-surface Q^3 sites and are correlated with intensity in the range of −113 to −114 ppm (orange lines, Roman numerals *vii–ix*; Figure 2) from covalently bonded Q^4 sites in the MFI zeolite nanosheets. Intensity correlations are also observed between pairs of Q^3 ^{29}Si signals at −99.7 and −102.5 ppm, at −101.1 and −103.6 ppm, and at −102.5 and −103.6 ppm (orange lines, Roman numerals *i–iii* in the boxed region of Figure 2), which establishes that their respective Q^3 moieties are covalently bonded, consistent with their mesopore surface locations.

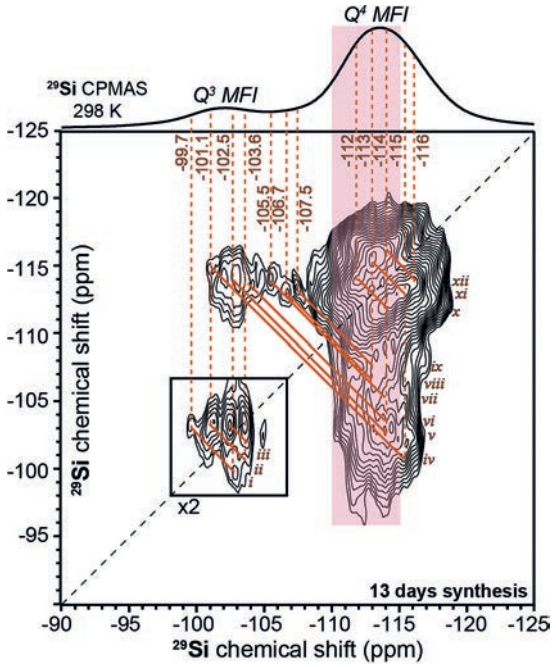

Figure 2. Solid-state 2D *J*-mediated (through-covalent-bond) ^{29}Si{^{29}Si} correlation spectrum of MFI zeolite nanosheets after 13 days of hydrothermal synthesis, enriched to 99% in ^{29}Si. The spectrum was acquired at 11.7 T, 298 K, and 12.5 kHz MAS. Pairs of correlated signal intensity are indicated by the solid orange anti-diagonal lines. The 2D *J*-mediated ^{29}Si{^{29}Si} correlation spectrum acquired at 95 K of the same material (Supporting Information, Figure S4) shows similar 2D ^{29}Si intensity correlations, which are similarly broadened and displaced under the same low-temperature conditions as used to acquire the DNP-NMR spectra in Figures 1b and 3a.

Most importantly, however, are the observations that the ^{29}Si signals from the Q^3 mesopore surface moieties of the MFI nanosheets (Figure 2) are correlated to those of the transforming nanolayered silicate moieties (Figures 1a,b, and Figure 3a). This is evident in the solid-state 2D DNP-enhanced *J*-mediated ^{29}Si{^{29}Si} spectrum in Figure 3a acquired at an earlier stage of crystallization (8.5 days) from the same batch and synthesized under identical composition and conditions, as for the sample measured in Figure 1 for a longer hydrothermal synthesis time (10 days). Figure 3a shows the same signals at −96.7, −102.4, −109, and −113 ppm (blue lines, Figure 3a) from the intermediate nanolayered silicate species as in Figure 1b, with higher overall intensities that reflect the lower extent of conversion to MFI nanosheets for the shorter hydrothermal synthesis time. Resolved 2D *J*-mediated ^{29}Si{^{29}Si} signals at −95.8, −97.7, −100.5, −101.3, −103.2, −105.3, and −107.8 ppm associated with transforming nanolayered silicate moieties are correlated with each other (green lines; Figure 3a) and signals in the range of −110 to −112 ppm (red lines; Figure 3a) from Q^4 species in the crystallizing MFI zeolite nanosheets. Several of these are especially noteworthy. In particular, the signals at −95.8 and −97.7 ppm from transforming nanolayered silicate site 1 moieties are correlated with the signals at −101.3 and −103.2 ppm from transforming site 2 and 3 moieties (Roman numerals *I* and *II*, thick green lines; Figure 3a), which are also each correlated with signal intensities at −110 and −112 ppm (Roman numerals *VI–IX*, thick red lines; Figure 3a) that arise from Q^4 species in the crystallizing MFI zeolite nanosheet framework. Similarly, the ^{29}Si signals at −100.5 and −101.3 ppm from transforming nanolayered silicate site 2 and 3 moieties are correlated with the signals at −105.3 and −107.8 ppm from transforming site 4 moieties (Roman numerals *III* and *IV*, thick green lines; Figure 3a), which are both also correlated with the signal at −112 ppm from the crystallizing MFI zeolite (Roman numerals *X* and *XI*, thick red lines; Figure 3a). The ^{29}Si signal at −100.5 ppm from transforming site 2 and 3 moieties is additionally correlated with the signal at −110 ppm from crystallizing MFI zeolite

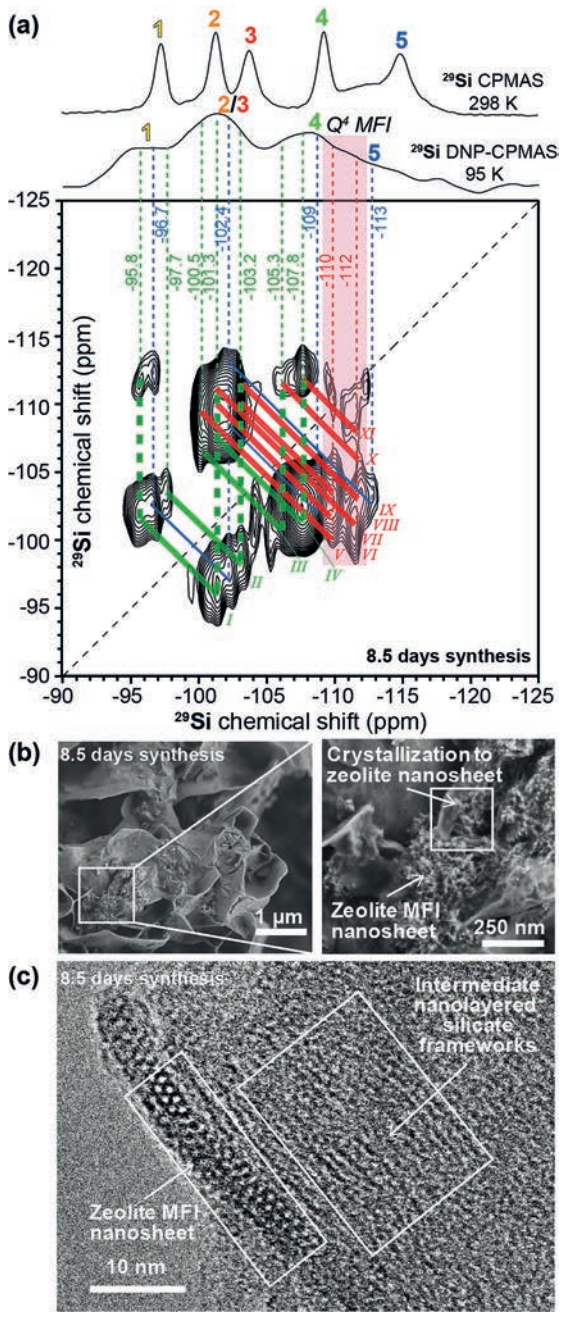

Figure 3. a) Solid-state 2D DNP-enhanced *J*-mediated (through-bond) $^{29}Si\{^{29}Si\}$ correlation spectrum of the intermediate product of crystallizing MFI zeolite nanosheets after 8.5 days of hydrothermal synthesis. The spectrum was acquired under the same conditions as in Figure 1b. For comparison, a 1D $^{29}Si\{^{1}H\}$ DNP-enhanced CPMAS spectrum acquired at the same conditions is shown, as is a 1D $^{29}Si\{^{1}H\}$ CPMAS spectrum acquired at 11.7 T, 298 K, and 12.5 kHz MAS. Pairs of correlated signals discussed in the text are indicated by the solid blue, red, and green anti-diagonal lines. Representative b) SEM images and c) TEM image showing regions in which intermediate nanolayered silicate sheets are transforming into MFI zeolite nanosheets.

(Roman numeral *V*, thick red line; Figure 3a). These correlated signals provide direct evidence for covalent ^{29}Si-O-^{29}Si bonding between the transforming nanolayered silicates and the mesostructured MFI zeolite nanosheets and their non-topotactic rearrangement during crystallization.

The 2D $^{29}Si\{^{29}Si\}$ NMR results for the 8.5 day sample are consistent with electron microscopy measurements that probe the morphologies and proximities of the intermediate nanolayered silicate and MFI zeolite nanosheet products. For example, the representative SEM images in Figure 3b show the flower-petal-like morphologies of the nanolayered silicates and the finer MFI zeolite nanosheets, both of which are intimately associated and with no evidence of macroscopically segregated products. The TEM image in Figure 3c, shows the nanoscale proximities of the MFI zeolite nanosheets and the transforming nanolayered silicates, similar to Figure 1c, but in a different local orientation. The 2D NMR results and electron microscopy observations are not consistent with the dissolution-reprecipitation mechanism or drying effects proposed by Goesten, et al., for which we have found no evidence under the conditions used.

Furthermore, contrary to the statement by Goesten, et al., the microscopy and 2D NMR analyses discussed above are consistent with the data trends of Tuel,[19] who studied layered silicate species that form during the syntheses of zeolites Beta and ZSM-48. Tuel found that the long-range order of intermediate nanolayered silicate frameworks, as measured by the intensity of the dominant basal reflection (at 6.2° 2θ, *d*-spacing of 1.4 nm) in the XRD patterns, appeared at early hydrothermal synthesis times, and then decreased as the synthesis progressed and zeolitic products crystallized. While different conditions were used in Ref. [19], our results are consistent with the same general trends. We also reported a marked decrease in long-range order (3° 2θ, *d*-spacings of 2.9 nm) associated with the nanolayered silicates between 8.5 and 10 days of hydrothermal synthesis, as shown in Figure 1 of Messinger, et al.[1] The greater *d*-spacing of the basal plane reflection compared to the system studied by Tuel reflects the longer chain length of the diquaternary-ammonium surfactant species.[1] The reduction of the long-range order is consistent with the rearrangement of the nanolayered silicates into MFI zeolite nanosheets and with the XRD results of Tuel.[19] Based on wide-angle XRD patterns only (> 5° 2θ, corresponding to a maximum *d*-spacing of 1.8 nm), Goesten, et al. report the absence of XRD reflections corresponding to nanolayered silicates in their efforts to synthetically reproduce our work, although the associated *d*-spacings would be outside the small-angle range required to detect the dominant first-order basal reflection from the nanolayered silicates. As reported in Messinger, et al.,[1] the wide-angle reflections associated with the *a*- and *b*-axes of the nanolayered silicates are weak and disappear upon crystallization of the MFI zeolite nanosheets; their detection likely requires the existence of a significant fraction of nanolayered silicate species, which Goesten, et al. do not find. They reject that temperature differences of ca. 20 °C in hydrothermal synthesis conditions (specifically, 130 °C versus 150 °C in an earlier study[20]) could result in the slower rate of MFI zeolite crystallization reported in Messinger, et al.[1] However, extensive reports in literature point to the contrary.[21–24] We cannot otherwise comment on the outcomes of specific syntheses about which we are not directly knowledgeable and which depend sensitively on synthesis compositions and conditions (e.g., pH, temperature, nanoscopic seed species).

In summary, all of the small- and wide-angle X-ray scattering, electron microscopy and 2D NMR data support the conclusion that, under the synthesis conditions used here and in Messinger, et al.,[1] the mesostructured MFI zeolite nanosheets form from nanolayered silicates that rearrange non-topotactically. In particular, the 2D ^{29}Si{^{29}Si} *J*-mediated NMR analyses establish unambiguously the covalent connectivities of transforming intermediate nanolayered silicate moieties and crystallizing mesostructured MFI zeolite nanosheets. We do not intend to imply that such non-topotactic transformations are universally general to zeolite syntheses and do not rule out that dissolution-recrystallization may contribute partially here (or under different synthesis conditions[25]). However, the 2D ^{29}Si{^{29}Si} *J*-mediated NMR results provide strong and direct evidence for non-topotactic rearrangement and condensation of a substantial fraction of the Q^3 and Q^4 Si T-sites in the nanolayered silicates during the mesostructured MFI zeolite crystallization process. In the present case, this is likely aided by the high density of partially condensed Q^3 moieties in the intermediate nanolayered silicates, as well as in the mesostructured MFI zeolite product. These analyses address the structural criticisms raised by Goesten, et al., which we consider to be without foundation. The measurements of structural rearrangements during crystallization of zeolites have been previously difficult to characterize, though are enabled in this case by the combination of high-spectral resolution and unprecedented sensitivity provided by newly available DNP-enhanced 2D *J*-mediated ^{29}Si{^{29}Si} NMR methods.

Acknowledgements

We thank Dr. S. Zones, Prof. Dr. L. McCusker, and Prof. Dr. C. Baerlocher for helpful discussions. This work was supported in part by the U.S. National Science Foundation under grant DMR-1429710 and by the Chevron Energy Technology Company. The NMR measurements were conducted using the Central Facilities of the UCSB Materials Research Laboratory, which are supported by the NSF MRSEC Program under award No. DMR-1121053; a member of the NSF-funded Materials Research Facilities Network (www.mrfn.org).

Conflict of interest

The authors declare no conflict of interest.

How to cite: *Angew. Chem. Int. Ed.* **2017**, *56*, 5164–5169
Angew. Chem. **2017**, *129*, 5246–5251

[1] R. J. Messinger, K. Na, Y. Seo, R. Ryoo, B. F. Chmelka, *Angew. Chem. Int. Ed.* **2015**, *54*, 927–931; *Angew. Chem.* **2015**, *127*, 941–945.

[2] D. H. Brouwer, R. J. Darton, R. E. Morris, M. H. Levitt, *J. Am. Chem. Soc.* **2005**, *127*, 10365–10370.
[3] D. H. Brouwer, P. E. Kristiansen, C. A. Fyfe, M. H. Levitt, *J. Am. Chem. Soc.* **2005**, *127*, 542–543.
[4] S. Cadars, M. Allix, D. H. Brouwer, R. Shayib, M. Suchomel, M. N. Garaga, A. Rakhmatullin, A. W. Burton, S. I. Zones, D. Massiot, B. F. Chmelka, *Chem. Mater.* **2014**, *26*, 6994–7008.
[5] S. C. Christiansen, D. Y. Zhao, M. T. Janicke, C. C. Landry, G. D. Stucky, B. F. Chmelka, *J. Am. Chem. Soc.* **2001**, *123*, 4519–4529.
[6] S. Cadars, D. H. Brouwer, B. F. Chmelka, *Phys. Chem. Chem. Phys.* **2009**, *11*, 1825–1837.
[7] S. Cadars, N. Mifsud, A. Lesage, J. D. Epping, N. Hedin, B. F. Chmelka, L. Emsley, *J. Phys. Chem. C* **2008**, *112*, 9145–9154.
[8] Q. Z. Ni, E. Daviso, T. V. Can, E. Markhasin, S. K. Jawla, T. M. Swager, R. J. Temkin, J. Herzfeld, R. G. Griffin, *Acc. Chem. Res.* **2013**, *46*, 1933–1941.
[9] T. Maly, G. T. Debelouchina, V. S. Bajaj, K. N. Hu, C. G. Joo, M. L. Mak-Jurkauskas, J. R. Sirigiri, P. C. A. van der Wel, J. Herzfeld, R. J. Temkin, R. G. Griffin, *J. Chem. Phys.* **2008**, *128*, 052211.
[10] A. J. Rossini, A. Zagdoun, M. Lelli, A. Lesage, C. Coperet, L. Emsley, *Acc. Chem. Res.* **2013**, *46*, 1942–1951.
[11] A. Lesage, M. Lelli, D. Gajan, M. A. Caporini, V. Vitzthum, P. Mieville, J. Alauzun, A. Roussey, C. Thieuleux, A. Mehdi, G. Bodenhausen, C. Coperet, L. Emsley, *J. Am. Chem. Soc.* **2010**, *132*, 15459–15461.
[12] P. Wolf, M. Valla, F. Nunez-Zarur, A. Comas-Vives, A. J. Rossini, C. Firth, H. Kallas, A. Lesage, L. Emsley, C. Coperet, I. Hermans, *ACS Catal.* **2016**, *6*, 4047–4063.
[13] R. P. Sangodkar, B. J. Smith, D. Gajan, A. J. Rossini, L. R. Roberts, G. P. Funkhouser, A. Lesage, L. Emsley, B. F. Chmelka, *J. Am. Chem. Soc.* **2015**, *137*, 8096–8112.
[14] D. Lee, G. Monin, N. T. Duong, I. Z. Lopez, M. Bardet, V. Mareau, L. Gonon, G. De Paepe, *J. Am. Chem. Soc.* **2014**, *136*, 13781–13788.
[15] P. Wolf, M. Valla, A. J. Rossini, A. Comas-Vives, F. Nunez-Zarur, B. Malaman, A. Lesage, L. Emsley, C. Coperet, I. Hermans, *Angew. Chem. Int. Ed.* **2014**, *53*, 10179–10183; *Angew. Chem.* **2014**, *126*, 10343–10347.
[16] W. R. Gunther, V. K. Michaelis, M. A. Caporini, R. G. Griffin, Y. Roman-Leshkov, *J. Am. Chem. Soc.* **2014**, *136*, 6219–6222.
[17] D. H. Brouwer, S. Cadars, J. Eckert, Z. Liu, O. Terasaki, B. F. Chmelka, *J. Am. Chem. Soc.* **2013**, *135*, 5641–5655.
[18] C. A. Fyfe, H. Grondey, Y. Feng, G. T. Kokotailo, *J. Am. Chem. Soc.* **1990**, *112*, 8812–8820.
[19] A. Tuel, *Chem. Mater.* **1999**, *11*, 1865–1875.
[20] M. Choi, K. Na, J. Kim, Y. Sakamoto, O. Terasaki, R. Ryoo, *Nature* **2009**, *461*, 246–249.
[21] A. Erdem, L. B. Sand, *J. Catal.* **1979**, *60*, 241–256.
[22] M. Ghamami, L. B. Sand, *Zeolites* **1983**, *3*, 155–162.
[23] R. J. Francis, D. O'Hare, *J. Chem. Soc. Dalton Trans.* **1998**, 3133–3148.
[24] C. S. Cundy, P. A. Cox, *Microporous Mesoporous Mater.* **2005**, *82*, 1–78.
[25] A. I. Lupulescu, J. D. Rimer, *Science* **2014**, *344*, 729–732.
[26] M. G. Goesten, X. Zhu, B. Mezari, E. J. M. Hensen *Angew. Chem. Int. Ed.* **2017**, *56* DOI: 10.1002/anie.201602856; *Angew. Chem.* **2017**, *129*, DOI: 10.1002/ange.201602856.

Manuscript received: October 12, 2016
Final Article published: April 5, 2017

Experimental Details

The synthesis and microscopy characterization methods of the siliceous MFI zeolite nanosheets and nanolayered silicate intermediate have been described previously.[1,2]

All solid-state DNP-enhanced $^{29}Si\{^{29}Si\}$ and $^{29}Si\{^{1}H\}$ NMR experiments were carried out on a Bruker ASCEND 400 DNP-NMR spectrometer with a 9.4 Tesla superconducting magnet operating at 399.95 and 79.46 MHz for ^{1}H and ^{29}Si nuclei, respectively, and equipped with a gyrotron and microwave transmission line capable of providing 263 GHz microwave irradiation at the sample and a low-temperature 3.2 mm MAS probe. The DNP-enhanced $^{29}Si\{^{1}H\}$ and $^{29}Si\{^{29}Si\}$ spectra were acquired at 95 K, 8 kHz MAS, under continuous microwave irradiation at 263 GHz, and in the presence of 16 mM TEKPol biradical[3] in frozen 1,1,2,2-tetrachloroethane (DNP solvent), which do not influence the structure of the material.[4] The ^{29}Si DNP NMR signal enhancements were quantified as the ratio of the fully-relaxed $^{29}Si\{^{1}H\}$ CPMAS signal intensities obtained with and without microwave irradiation, which was measured to be ca. 9 and 23 for the intermediate products obtained after 10 and 8.5 days of hydrothermal synthesis, respectively. Solid-state 2D DNP-enhanced *J*-mediated $^{29}Si\{^{29}Si\}$ spectra[5,6] were acquired using $^{29}Si\{^{1}H\}$ cross-polarization with a contact time of 4 ms to circumvent the effects of the long longitudinal ^{29}Si spin relaxation times. An experimentally optimized half-spin-echo (τ) delay of 16 ms and a repetition time of 8.5 s were used for best overall efficiency.

The solid-state 2D *J*-mediated $^{29}Si\{^{29}Si\}$ spectrum of MFI zeolite nanosheets after 13 days of hydrothermal synthesis, isotopically enriched to 99% abundance in ^{29}Si, was acquired on a Bruker AVANCE IPSO 500 NMR spectrometer with an 11.74 Tesla widebore superconducting magnet operating at 500.13 and 99.35 MHz for ^{1}H and ^{29}Si nuclei, respectively. The spectrum was acquired at 298 K, using $^{29}Si\{^{1}H\}$ cross-polarization with a contact time of 4 ms, with an experimentally-optimized τ delay of 5 ms, and a repetition time of 1.2 s.

Temperature dependences of ^{29}Si NMR chemical shifts and linewidths in surfactant-templated mesostructured silicates

The ^{29}Si signals from the transforming nanolayered silicate species in the intermediate products of crystallizing MFI zeolite nanosheets (Figs. 1a,b, 3a, and S3) exhibit temperature-

dependent positions and linewidths, which are consistent with past results reported for surfactant-templated mesostructured silicates. Specifically, Cadars, et al.[6] have previously shown that the bulk neat surfactant-templated nanolayered silicate exhibits ^{29}Si MAS NMR signals from five distinct framework sites with positions and linewidths that vary over the range 205-328 K, due to temperature-dependent interactions of the framework silicate sites with the surfactant structure-directing species. For example, the 2D *J*-mediated ^{29}Si{^{29}Si} spectra acquired at 298 K (Fig. S1a, black) of the bulk neat nanolayered silicate, which was synthesized separately from the intermediate products of MFI zeolite crystallization, shows well-resolved ^{29}Si signal pairs arising from covalent connectivities among the five framework sites, as previously discussed.[6] By contrast, in the 2D *J*-mediated ^{29}Si{^{29}Si} correlation spectrum acquired at 278 K (Fig. S1a, red), the same signals are broadened due to distributions of local ^{29}Si environments that arise from the freezing out of motions of the surfactant structure-directing agent, though the covalent site connectivities of the silicate framework are unaffected. Similar interactions are expected to contribute to and account for the broadening of the ^{29}Si signal linewidths in the DNP-enhanced spectra of the intermediate products of crystallizing MFI zeolite nanosheets in Figs. 1b, 3a, S3, and S4, which were acquired under low temperature conditions (95 K).

Compared to otherwise identical spectra acquired at room temperature, all five ^{29}Si signals from bulk neat nanolayered silicate broaden and are displaced, as shown in the variable-temperature ^{29}Si{^{1}H} CPMAS spectra in Fig. S1b acquired over the temperature range 205-328 K.[6] Whereas the ^{29}Si signals associated with sites 1, 4, and 5 broaden but remain resolved, the ^{29}Si signals from nanolayered silicate sites 2 and 3 overlap at temperatures below ca. 253 K. Below this temperature, the surfactant dynamics are effectively frozen and further reductions in temperature do not lead to significant further ^{29}Si signal broadening. The ^{29}Si signals from bulk neat nanolayered silicate in the DNP-enhanced spectra in Figs. S2 and S3 and discussed below, have similar positions and linewidths as those in the 1D ^{29}Si{^{1}H} CPMAS spectrum acquired at 205 K.

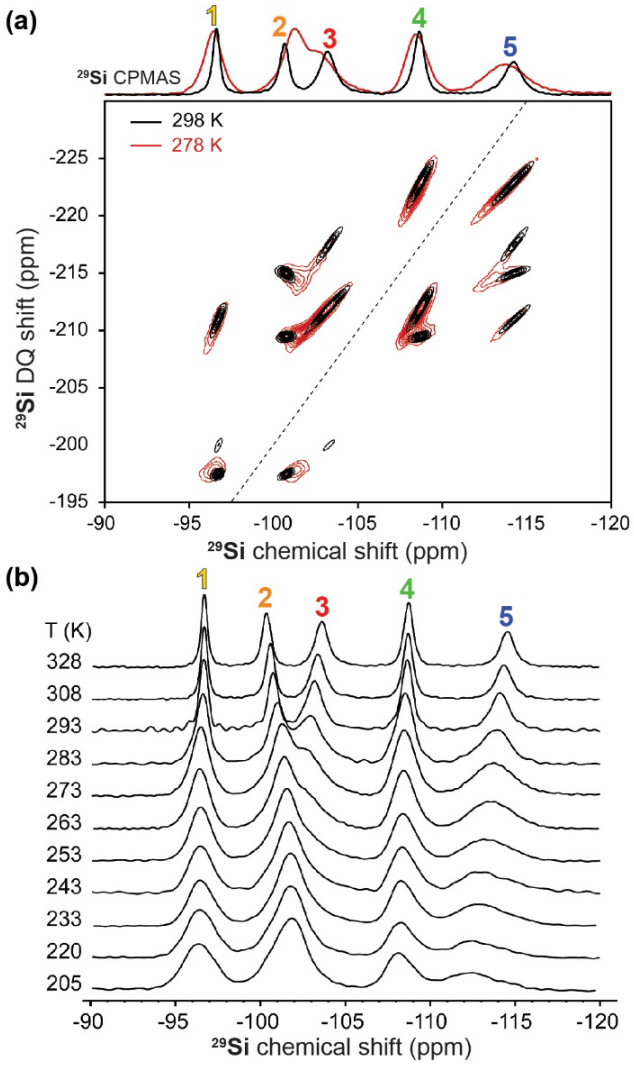

***Figure S1*. (a)** Solid-state 2D *J*-mediated $^{29}Si\{^{29}Si\}$ correlation spectra acquired at 298 K (black) and 278 K (red) of a $CH_3(CH_2)_{15}N^+(CH_3)_2(CH_2CH_3)$ surfactant-templated nanolayered silicate, enriched partially to 50% ^{29}Si. The spectra are overlain as 2D contour plots with single- and double-quantum ^{29}Si shift axes on the abscissa and ordinate, respectively, with pairs of ^{29}Si signals arising from the five distinct ^{29}Si sites in the nanolayered silicate coordinated across the 2:1 diagonal (black dashed line). The ^{29}Si signals from the five distinct sites in the nanolayered silicate broaden at low temperatures, due to broader distributions of local site environments that arise from the freezing out of motions of the surfactant structure-directing agent. **(b)** Temperature-dependent ^{29}Si CP-MAS NMR spectra of the same surfactant-templated nanolayered silicate as in (a) over the temperature range 205-328 K. The ^{29}Si signals broaden and are displaced at lower temperatures. Adapted from Cadars, et al., *J. Phys. Chem. C* **2008**, *112*, 9145-9154, ref. [6].

Physical mixture of bulk neat nanolayered silicate and bulk final (13 day) MFI zeolite nanosheet product

To make clearer the key correlated intensities in the 2D DNP-enhanced *J*-mediated $^{29}Si\{^{29}Si\}$ NMR spectra in Fig. 1b and 3a, we conducted complementary measurements on a simple physical mixture of bulk neat nanolayered silicate and the final product of MFI zeolite nanosheet crystallization after 13 days of hydrothermal synthesis. The bulk neat surfactant-templated nanolayered silicate was prepared in a separate synthesis, as described previously,[6] with 50% ^{29}Si isotopic enrichment for improved sensitivity (same sample as Fig. S1), and the bulk MFI zeolite nanosheet product after 13 days of hydrothermal synthesis was prepared with 99% ^{29}Si isotopic enrichment (same sample as Figs. 2 and S4). A simple physical mixture of the two bulk materials was prepared by combining and gently mixing ca. 1 mg of the final MFI zeolite nanosheet product with ca. 5 mg of the bulk neat nanolayered silicate, which was estimated to provide approximately equal ^{29}Si signal intensities from the two materials. The 2D DNP-enhanced *J*-mediated $^{29}Si\{^{29}Si\}$ spectrum acquired at 95 K of the resulting physical mixture (Fig. S2) shows resolved correlated ^{29}Si signal pairs at (-96.7 ppm, -102.4 ppm), (-102.4 ppm, 108.8 ppm), and (-102.4 ppm, -113 ppm) from the five distinct sites in the nanolayered silicates (blue lines). The signals are broadened and displaced at the low temperature conditions (95 K), as expected from the results of Cadars, et al.[6] and as discussed above (Fig. S1). Additional pairs of correlated ^{29}Si signal intensities at (-99.8 ppm, -101.4 ppm), (-99.8 ppm, -103.1 ppm), and (-101.4 ppm, -111 ppm) are detected from Q^3 sites on the surfaces of the MFI zeolite nanosheets and at (-111 ppm, -112 ppm) and (-110 ppm, -111 ppm) from Q^4 sites in the MFI zeolite framework (orange lines). These intensity correlations are consistent with the 2D *J*-mediated $^{29}Si\{^{29}Si\}$ correlation spectra of the MFI zeolite nanosheets alone after 13 days of hydrothermal synthesis (Figs. 2 and S4). While the ^{29}Si signals from sites 2 and 3 in the nanolayered silicates overlap the spectral region for the Q^3 sites in the final MFI zeolite product, the ^{29}Si signals from the nanolayered silicate are nevertheless relatively narrow (ca. 2.5 ppm FWHM), compared to the broad (ca. 6 ppm FWHM) ^{29}Si signal intensities from Q^3 sites in the final MFI zeolite product. There are no additional ^{29}Si signals that could be assigned to transforming nanolayered silicate species or covalent interactions between the nanolayered silicates and the final MFI zeolite product.

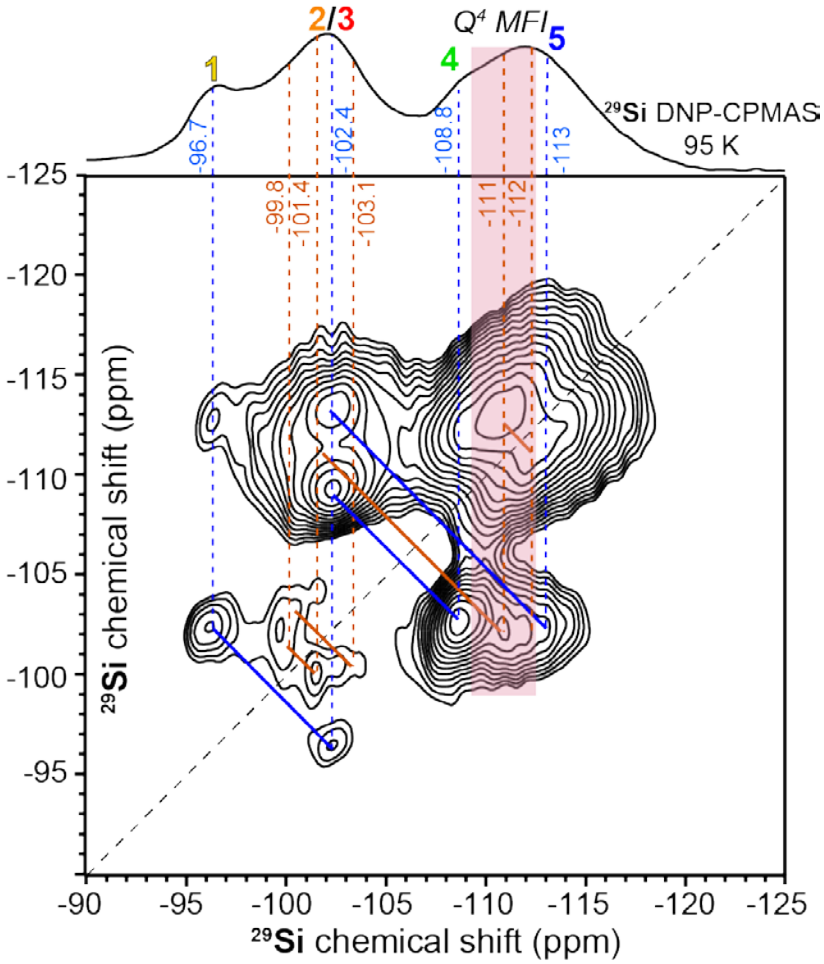

Figure S2. Solid-state 2D DNP-enhanced *J*-mediated ^{29}Si{^{29}Si} correlation spectrum of a physical mixture of nanolayered silicate (ca. 5 mg, same sample as in Fig. S1) and MFI zeolite nanosheets after 13 days of hydrothermal synthesis (ca. 1 mg, same sample as in Fig. 2), acquired at 9.4 T, 95 K, 8 kHz MAS, in the presence of 16 mM TEKPol biradical in frozen tetrachloroethane (DNP solvent), and under microwave irradiation at 263 GHz. Correlated ^{29}Si signals from the five distinct sites in the nanolayered silicate (blue lines) are resolved from the signals from the crystalline MFI zeolite nanosheets (orange lines), and as expected, there is no evidence of covalent interactions between the physically-mixed species.

Comparison of the physical mixture of bulk neat nanolayered silicate and bulk final (13 day) MFI zeolite nanosheet product with intermediate (8.5 day) crystallizing MFI zeolite nanosheets

Compared to the 2D DNP-enhanced *J*-mediated $^{29}Si\{^{29}Si\}$ spectrum of the physical mixture in Figure S2, clear differences are observed in the corresponding spectrum acquired for the intermediate (8.5 day) crystallizing MFI zeolite nanosheets. Additional intensity correlations are observed in the intermediate crystallization product that reflect the covalent linkages between transforming nanolayered silicate moieties and the crystallizing MFI zeolite nanosheets. These differences are clearly seen in Fig. S3, which overlays the 2D DNP-enhanced *J*-mediated $^{29}Si\{^{29}Si\}$ correlation spectrum of the physical mixture (black, same spectrum as in Fig. S2) with the corresponding spectrum of the intermediate (8.5 day) crystallizing MFI zeolite nanosheets (burgundy, same spectrum as in Fig. 3a). In both spectra, 2D ^{29}Si signal pairs are detected at (-96.7 ppm, -102.4 ppm), (-102.4 ppm, -109 ppm), and (-102.4 ppm, -113 ppm) from nanolayered silicate species (blue lines), as well as partially-resolved ^{29}Si signals in the shift range -110 to -112 ppm from Q^4 sites in the MFI zeolite (red band). Additionally, in the burgundy-colored spectrum of the crystallizing MFI zeolite nanosheets only, additional 2D ^{29}Si signal intensities are detected from the transforming nanolayered silicates (dashed green lines) which are correlated with each other (solid green lines) and with the crystallizing MFI zeolite nanosheets (solid red lines), as discussed in the main text. Notably, the signals from the transforming nanolayered silicate sites at -95.8, -101.3, and -109 ppm are broader (ca. 3.5 ppm FWHM) and displaced by ca. 1 ppm, compared to the signals from the untransformed nanolayered silicates. These correlated signal intensities, which are absent in the corresponding spectrum of the simple physical mixture, establish the presence of distributions of locally-distinct ^{29}Si sites in the transforming nanolayered silicate intermediates that are covalently bonded to the crystallizing MFI zeolite nanosheets. Such correlated ^{29}Si pairs of signals provide direct evidence for covalent ^{29}Si-O-^{29}Si bonding between transforming nanolayered silicate intermediates and the MFI zeolite nanosheets and their non-topotactic rearrangement during the hydrothermal crystallization process.

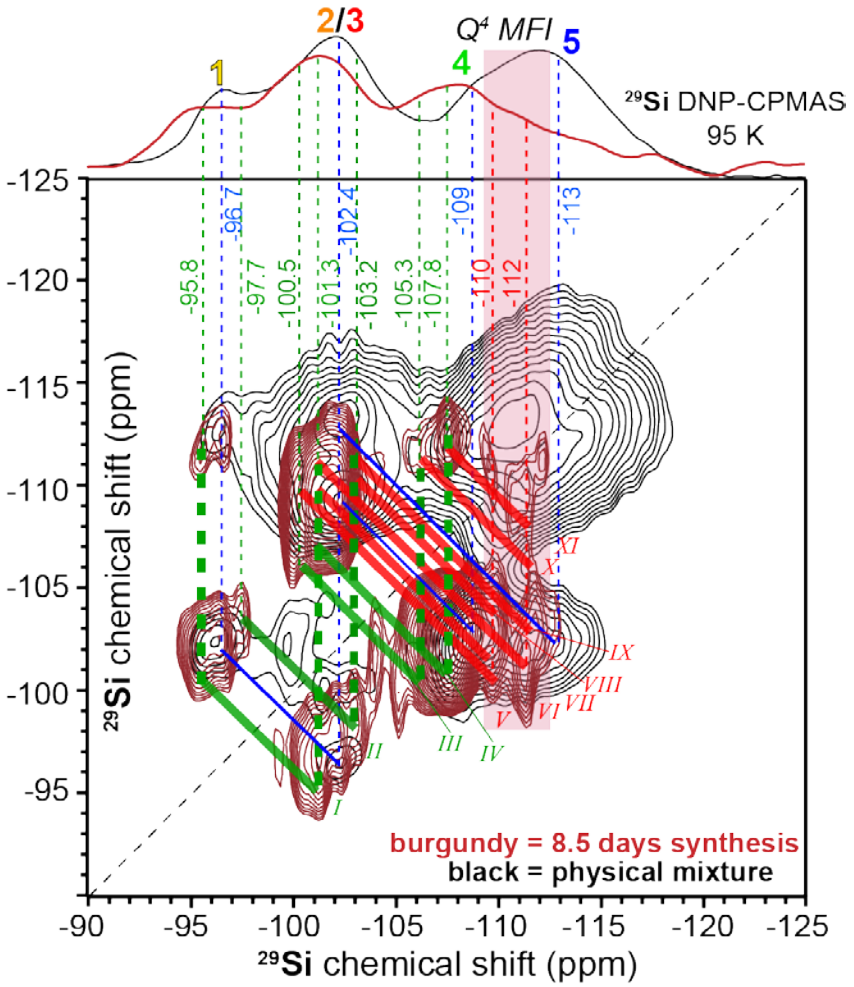

Figure S3. An overlay of the 2D DNP-enhanced *J*-mediated ^{29}Si{^{29}Si} correlation spectrum in Fig. S2 of the physical mixture of nanolayered silicate and fully-crystalline MFI zeolite (black) and the 2D spectrum in Fig. 3a (burgundy) of crystallizing MFI zeolite nanosheets after 8.5 days of hydrothermal synthesis. Signals from the five distinct silicate sites in the nanolayered silicates are clearly present in both spectra (dashed blue lines). Crucially, in the crystallizing MFI zeolite nanosheets, additional correlated ^{29}Si signals are resolved from transforming nanolayered silicate species (dashed green lines) and from the crystallizing MFI zeolite nanosheets (dashed red lines) which establish their covalent connectivities as discussed in the text. In particular, the signals at -95.8 and -97.7 ppm from transforming nanolayered silicate site 1 moieties are correlated with the signals at -101.3 and -103.2 ppm from transforming sites 2 and 3 moieties (Roman numerals *I* and *II,* thick green lines), which are also each correlated with signal intensities at -110 and -112 ppm (Roman numerals *VI-IX,* thick red lines) that arise from Q^4 species in the crystallizing MFI zeolite nanosheet framework. Similarly, the ^{29}Si signals at -100.5 and -101.3 ppm from transforming nanolayered silicate sites 2 and 3 moieties are correlated with the signals at -105.3 and -107.8 ppm from transforming site 4 moieties (Roman numerals *III* and *IV*, thick green

lines), the latter of which are both also correlated with the signal at -112 ppm from the crystallizing MFI zeolite (Roman numerals *X* and *XI*, thick red lines). The ^{29}Si signal at -100.5 ppm from transforming site 2 and 3 moieties is additionally correlated with the signal at -110 ppm from crystallizing MFI zeolite (Roman numeral *V*, thick red line). These correlated signals provide direct evidence for covalent ^{29}Si-O-^{29}Si bonding between the transforming nanolayered silicates and the mesostructured MFI zeolite nanosheets and their non-topotactic rearrangement during crystallization. By comparison, none of these correlated intensities are observed in the spectrum of the physical mixture of nanolayered silicate and MFI zeolite nanosheets.

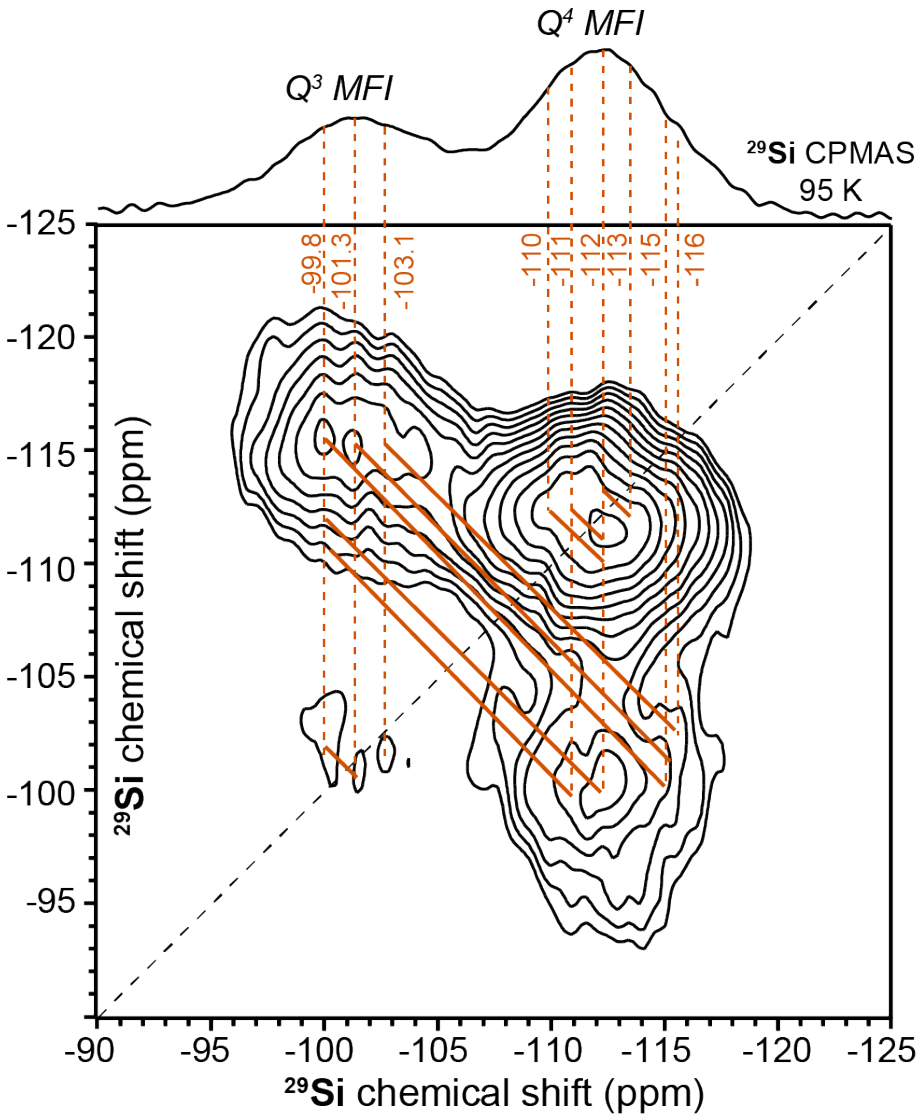

Figure S4. Solid-state 2D *J*-mediated (through-covalent-bond) ^{29}Si{^{29}Si} correlation spectrum of MFI zeolite nanosheets after 13 days of hydrothermal synthesis, isotopically enriched to 99% abundance in ^{29}Si (same sample as in Fig. 2). Similar signals as in Fig. 2 are detected (orange lines), though which are broadened and displaced under the same low-temperature conditions used for comparison with the DNP-NMR spectra in Figures 1b, 3a, S2, and S3.

Supporting Information references

[1] K. Na, M. Choi, W. Park, Y. Sakamoto, O. Terasaki, R. Ryoo, *J. Amer. Chem. Soc.* **2010**, *132*, 4169-4177.

[2] R. J. Messinger, K. Na, Y. Seo, R. Ryoo, B. F. Chmelka, *Angew. Chem. Int. Ed.* **2015**, *54*, 927-931.

[3] A. Zagdoun, G. Casano, O. Ouari, M. Schwarzwalder, A. J. Rossini, F. Aussenac, M. Yulikov, G. Jeschke, C. Coperet, A. Lesage, P. Tordo, L. Emsley, *J. Amer. Chem. Soc.* **2013**, *135*, 12790-12797.

[4] R. P. Sangodkar, B. J. Smith, D. Gajan, A. J. Rossini, L. R. Roberts, G. P. Funkhouser, A. Lesage, L. Emsley, B. F. Chmelka, *J. Amer. Chem. Soc.* **2015**, *137*, 8096-8112.

[5] A. Lesage, M. Bardet, L. Emsley, *J. Amer. Chem. Soc.* **1999**, *121*, 10987-10993.

[6] S. Cadars, N. Mifsud, A. Lesage, J. D. Epping, N. Hedin, B. F. Chmelka, L. Emsley, *J. Phys. Chem. C* **2008**, *112*, 9145-9154.